Hyperentangled photon sources in semiconductor waveguides

Dongpeng Kang,[1,2,*] L. G. Helt,[2,3,†] Sergei V. Zhukovsky,[1,2,3,‡] Juan P. Torres,[4,5] J. E. Sipe,[2,3] and A. S. Helmy[1,2]

[1]*The Edward S. Rogers Department of Electrical and Computer Engineering, University of Toronto, 10 King's College Road, Toronto, Ontario, Canada M5S 3G4*

[2]*Institute for Optical Sciences, University of Toronto, 60 St. George Street, Toronto, Ontario, Canada M5S 3G4*

[3]*Department of Physics, University of Toronto, 60 St. George Street, Toronto, Ontario, Canada M5S 1A7*

[4]*ICFO-Institut de Ciencies Fotoniques, Mediterranean Technology Park, 08860 Castelldefels (Barcelona), Spain*

[5]*Departament of Signal Theory and Communications, Universitat Politecnica de Catalunya, 08034 Barcelona, Spain*

We propose and analyze the performance of a technique to generate mode and polarization hyperentangled photons in monolithic semiconductor waveguides using two concurrent type-II spontaneous parametric down-conversion (SPDC) processes. These two SPDC processes are achieved by waveguide engineering which allows for simultaneous modal phase matching with the pump beam in a higher-order mode. Paired photons generated in each process are cross polarized and guided by different guiding mechanisms, which produces entanglement in both polarization and spatial mode. Theoretical analysis shows that the output quantum state has a high quality of hyperentanglement by spectral filtering with a bandwidth of a few nanometers, while off-chip compensation is not needed. This technique offers a path to realize an electrically pumped hyperentangled photon source.

PACS number(s): 42.65.Lm, 03.67.Bg, 42.50.Dv, 42.82.Et

I. INTRODUCTION

Paired photons that are entangled in multiple degrees of freedom (DOFs), or hyperentangled, have attracted a lot of interest in recent years [1–4]. Due to the presence of quantum correlations in several DOFs, they offer significant advantages in quantum information processing, in particular in tasks such as superdense coding, multidimensional quantum cryptography, and the efficient construction of cluster states.

In superdense coding, for example, paired photons simultaneously entangled in polarization (spin) and orbital angular momentum were shown to provide a channel capacity that exceeds the limit of standard quantum dense coding with linear optics [5]. In addition to the applications mentioned above, hyperentangled photons can also enhance the degree of violation of Bell's-like inequalities [6] and reduce the detection efficiency required for closing the detection loophole in Bell tests [7].

The most extensively used method to produce entangled or hyperentangled photons is via the nonlinear optical process of spontaneous parametric down-conversion (SPDC) in nonlinear crystals with a second-order susceptibility $\chi^{(2)}$. Photon pairs generated via SPDC have many DOFs available, such as frequency, temporal location, linear momentum, spatial shape (orbital angular momentum), and polarization. Even though different types of nonlinear crystals have been used for generating paired photons via SPDC, driven by the demand for high-efficiency single and two-photon sources, and the need for on-chip integration of quantum computing, there has

been a focus on periodically poled lithium niobate (PPLN) and potassium titanyl phosphate (PPKTP) waveguides. This class of sources makes use of quasi phase matching (QPM) to provide access to the highest nonlinear coefficient of the material [8]. In these waveguide sources, the photon pair generation rates are increased by orders of magnitude over their bulk crystal counterparts, and the use of well-confined waveguide modes makes the collection of generated photons in optical circuits easier.

To date, energy-time and polarization entanglement have been demonstrated using these waveguide sources in various configurations [8]. Hyperentanglement has not been demonstrated so far. However, it has been proposed that some higher-order spatial modes of these waveguides could be used to produce and manipulate modal and hyperentangled photons on a chip [9,10]. Moreover, experimental progress has been reported on the use of spatial modes of different orders in SPDC using waveguide devices [11–13].

While the use of PPLN and PPKTP waveguides certainly provide an interesting platform for studying quantum nonlinear optics, these ferroelectric materials cannot be monolithically integrated with photonics devices with complex functions or pump lasers on the same chip, hindering further on-chip integration. To this end, the III-V semiconductor system GaAs/AlGaAs is a promising alternative. These structures can be integrated with both active and passive photonic components. Various strategies have been developed to achieve phase matching (PM) in AlGaAs waveguides [14,15]: QPM [16–18], form birefringence [19,20], modal phase matching (MPM) [21], counterpropagating modes [22], and the use of Bragg reflection waveguides (BRWs) [23,24]. Techniques to generate polarization entangled photons in AlGaAs waveguides have been theoretically developed [25–27] as well as experimentally demonstrated [22,28,29].

In this work, we propose and analyze a technique that utilizes phase matching in Bragg reflection waveguides to produce hyperentangled photons. Paired photons are generated concomitantly utilizing two type-II SPDC processes: the first

---

*dongpeng.kang@mail.utoronto.ca

†Current address: Centre for Ultrahigh bandwidth Devices for Optical Systems (CUDOS), MQ Photonics Research Centre, Department of Physics and Astronomy, Faculty of Science, Macquarie University, NSW 2109, Australia.

‡Current address: DTU Fotonik, Department of Photonics Engineering, Technical University of Denmark, Ørsteds Plads 343, DK-2800 Kgs. Lyngby, Denmark.

SPDC process generates a photon in a TE Bragg reflection guided (Bragg) mode and one in a TM total internal reflection (TIR) guided mode, while the second SPDC process generates a photon in a TM Bragg mode and one in a TE TIR mode. The novelty in this scenario consists in achieving modal entanglement via spatial modes with different guiding mechanisms, which can be tailored by waveguide structure engineering with much greater flexibility compared to spatial modes with the same guiding mechanism but of different orders used in previous studies. By spectrally separating the two photons of a pair, photons hyperentangled in modal and polarization DOFs can be produced. Such a technique provides a viable route for electrically pumped on-chip generation and manipulation of hyperentangled photons.

II. OBTAINING HYPERENTANGLEMENT IN BRAGG REFLECTION WAVEGUIDES

BRWs are a class of one-dimensional photonic band-gap structures that use Bragg reflections from periodic stacks of layers to provide optical confinement of light [30]. The modal dispersion properties of Bragg modes are distinct from those of TIR modes, and can be tuned to a large extent by modifying the layer structure. BRWs can also be designed such that they simultaneously support both Bragg modes and TIR modes. Thanks to this controllable modal dispersion, BRWs have gained much interest as waveguide SPDC photon sources. Designs have considered achieving phase matching by pumping the Bragg mode and generating photons in TIR modes [31], as well as employing QPM such that one of the photons in a pair is generated in the Bragg mode, while its twin is generated in the TIR mode. In this second configuration the large tunability of the Bragg mode can be used to generate quantum separable states as a resource for pure heralded single photons [32].

In each of these PM schemes, it is generally advantageous to use a type-II SPDC process so that the paired photons can be conveniently separated according to their polarization, rather than according to their mode or energy. For example, BRWs can be designed to generate paired photons in a TE polarized Bragg mode and a TM polarized TIR mode. In such a case, however, there coexists another type-II process which generates paired photons in a TM Bragg mode and a TE TIR mode. Although the two processes usually have slightly different PM wavelengths, photon pairs can still be simultaneously generated from the second process and thus pollute the desired photon pairs from the first process. This issue is especially critical when the waveguide is pumped by ultrashort pulses with a spectral bandwidth larger than the difference between the PM wavelengths of both processes, which is usually a few nanometers. Therefore, BRWs of this category should be designed to have a significant PM wavelength difference between the two type-II processes.

On the other hand, it is possible to design a BRW for which the two processes have identical PM wavelengths, and paired photons with similar spectra are generated via the two processes with nearly equal probabilities. These photons are hyperentangled in frequency, mode, and polarization.

Achieving hyperentanglement in this fashion has several advantages over techniques that use higher-order spatial modes in ferroelectric waveguides [9,10]. First, it allows for monolithic integration. Second, the mature epitaxial growth and nanofabrication techniques available for AlGaAs allow accurate modeling of the designed devices, whereas ferroelectric waveguides, usually fabricated by ion exchange and having diffused index profiles, cannot provide the fabrication tolerances required by concurrent PM. Moreover, birefringent ferroelectric materials cause significant phase distinguishability in any type-II process, thus reducing the measured visibility in Hong-Ou-Mandel–type experiments unless off-chip phase compensation is carried out. In AlGaAs BRWs, however, the modal birefringences can be engineered at will and may be designed to be small enough such that a high visibility can be obtained with practical spectral filtering rather than phase compensation, as will be demonstrated and discussed further below.

III. WAVEGUIDE STRUCTURES FOR HYPERENTANGLEMENT

To better illustrate the hyperentanglement generation technique introduced in the previous section, we give an illustrative example. Instead of using QPM [32], we choose MPM with the pump being in a higher-order spatial mode. This is because QPM in AlGaAs waveguides is challenging: it is difficult to periodically modulate the material, and doing so leads to increased losses. MPM, on the other hand, can be simply achieved lithographically in ridge waveguides.

For example, a BRW is designed to PM a pump beam in the TE_{40} mode at around 775 nm. In SPDC process 1, paired photons are generated in a TE [horizontal (H)] Bragg mode (B) (signal photon, denoted HB) and a TM [vertical (V)] TIR mode (T) (idler photon, denoted VT). In SPDC process 2, paired photons are generated in a TM Bragg mode (signal photon, denoted VB) and a TE TIR mode (idler photon, denoted HT). Along the epitaxial (y) direction, the waveguide has a 1061-nm-thick high-index core of $Al_{0.2}Ga_{0.8}As$ above a Bragg mirror consisting of six pairs of 742 nm $Al_{0.65}Ga_{0.35}$ As/301 nm $Al_{0.2}Ga_{0.8}As$. Above the core, there is a 300 nm layer of $Al_{0.4}Ga_{0.6}As$ used to increase the modal overlaps of both processes. On top of the structure is a layer of 2.21 μm low-index cladding made of $Al_{0.8}Ga_{0.2}As$.

The thickness of the core layer is determined by the waveguide dispersion relation required for the HB mode, obtained from the transfer matrix method, while the thicknesses of the layers making up the Bragg mirror are determined by quarter-wave conditions which place the HB mode in the center of the photonic band gap. The design equations can be found in Abolghasem *et al.* [33]. Schematics of the epitaxial structure and the refractive index profile are shown in Figs. 1(a) and 1(b), respectively. In such a structure, HB and VB modes are confined by Bragg reflections from the lower side of the core, and TIRs from the upper side. Meanwhile, the structure simultaneously supports HT and VT modes at both down-converted and pump wavelengths. A single-sided BRW [33], rather than a conventional symmetrical BRW, is used to decrease the etch depth needed to provide sufficient lateral modal confinement and to ease fabrication challenges.

The PM condition requires the effective indices of the pump mode (p), and down-converted modes (α) and (β) to satisfy $2n_{\text{eff},p}(\omega_p) = n_{\text{eff},\alpha}(\omega_p/2) + n_{\text{eff},\beta}(\omega_p/2)$. This is why
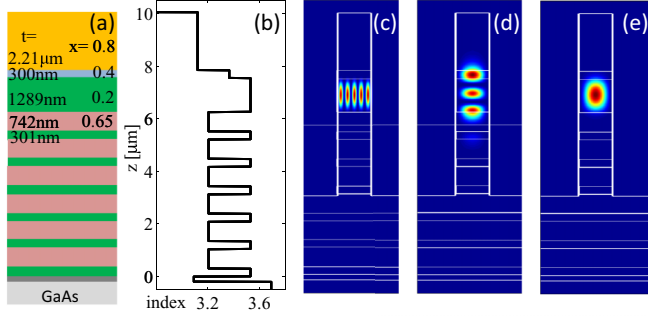
FIG. 1. (Color online) (a) Epitaxial structure of the waveguide, with layer thicknesses t and aluminum concentrations x; (b) vertical refractive index profile at 775 nm; (c)–(e) modal intensity profiles for the pump TE$_{40}$ mode, down-converted TE Bragg mode, and TE TIR mode, respectively. The TM Bragg and TM TIR modes have similar profiles and are not shown here.

we choose the pump mode to be TE$_{40}$, and use a deep etched waveguide with an etch depth of ∼7 μm. The modal intensity profiles are shown in Figs. 1(c)–1(e). As the ridge width decreases, the effective index of the pump mode decreases much faster than those of the generated photon modes. As can be seen from Fig. 2(a), when the ridge width $W \approx 1$ μm, the PM condition can be roughly satisfied for both processes. However, according to Fig. 2(b), the ridge widths required for the two processes are slightly different, thus a fixed ridge width will lead to different PM wavelengths for the two processes.

To align the two PM wavelengths, the modal birefringences should satisfy $n_{\text{eff},HB}(\omega_p/2) - n_{\text{eff},VB}(\omega_p/2) = n_{\text{eff},HT}(\omega_p/2) - n_{\text{eff},VT}(\omega_p/2)$. An earlier study [34] has shown that the birefringence of BRWs can be tuned by changing the core thickness or the thicknesses of the high-index and low-index

layers in the Bragg mirror. Here we change the core thickness and find the corresponding PM wavelengths. The dependence of the PM wavelength difference $\Delta\lambda_{\text{PM}} = \lambda_{\text{PM2}} - \lambda_{\text{PM1}}$ on the core thickness is shown in Fig. 2(b), for a ridge width $W = 1.08$ μm. When $t_c = 1289$ nm, concurrent PM is achieved at 1550.7 nm. Therefore, the structure designed here supports two type-II SPDC processes at the same PM wavelength, allowing generation of hyperentangled photons.

IV. PERFORMANCE ANALYSIS

In this section, we investigate the properties of the paired photons generated in the waveguide structure designed above. Following the backward Heisenberg picture approach of [35,36], under the undepleted pump approximation and with a low probability of pair production, the quantum state of the Hilbert space involving signal and idler photons can be written as $|\Psi_{\text{gen}}\rangle \approx |\text{vac}\rangle + \nu|II\rangle$, where

$$|II\rangle = \frac{1}{\sqrt{2}} \int d\omega_1 d\omega_2 \sum_{\alpha,\beta} \phi_{\alpha\beta}(\omega_1,\omega_2) a_\alpha^\dagger(\omega_1) a_\beta^\dagger(\omega_2)|\text{vac}\rangle \tag{1}$$

is the normalized two-photon state. The biphoton wave function (BWF) $\phi_{\alpha\beta}(\omega_1,\omega_2)$ is

$$\phi_{\alpha\beta}(\omega_1,\omega_2) = F_{\alpha\beta}(\omega_1,\omega_2)\phi_P(\omega_1 + \omega_2), \tag{2}$$

where

$$F_{\alpha\beta}(\omega_1,\omega_2) = iL\sqrt{\frac{dk_\alpha(\omega_1)}{d\omega_1}}\sqrt{\frac{dk_\beta(\omega_2)}{d\omega_2}}$$

$$\times \left(\sqrt{\frac{dk_p(\omega)}{d\omega}}\right)_{\omega=\omega_1+\omega_2}\sqrt{\frac{\omega_1\omega_2(\overline{\chi}_2)^2|\mu|^2}{8\pi\varepsilon_0|\nu|^2\overline{n}^6}}$$

$$\times \sqrt{\frac{\hbar(\omega_1+\omega_2)}{\mathcal{A}[k_\alpha(\omega_1),k_\beta(\omega_2),k_p(\omega_1+\omega_2)]}}$$

$$\times \text{sinc}\left(\frac{\Delta k_{\alpha\beta}(\omega_1,\omega_2)L}{2}\right).$$

Here the Greek subscripts α, β label the generated photon modes (HB, VB, HT, VT); $|\mu|^2$ is the average number of photons in the pump pulse; $\phi_P(\omega)$ is the pump pulse amplitude; L is the length of the waveguide; $\overline{n}$ and $\overline{\chi}_2$ are typical values of the refractive index and the second-order optical nonlinearity, respectively, introduced solely for convenience and do not affect the efficiency calculation [35]. The function $\Delta k_{\alpha\beta} = k_\alpha(\omega_1) + k_\beta(\omega_2) - k_p(\omega_1 + \omega_2)$ is the phase-matching function, and

$$\mathcal{A}[k_\alpha(\omega_1),k_\beta(\omega_2),k_p(\omega_1+\omega_2)]$$

$$= \left| \int dx\,dy \frac{\overline{n}^3 \chi_2^{ijk}(x,y)}{\overline{\chi}_2} \right.$$

$$\left. \times \frac{[d_{k_\alpha(\omega_1)}^i(x,y)]^*[d_{k_\beta(\omega_2)}^j(x,y)]^* d_{k_p(\omega_1+\omega_2)}^k(x,y)}{\varepsilon_0^{3/2} n^2(x,y;\omega_1)n^2(x,y;\omega_2)n^2(x,y;\omega_1+\omega_2)} \right|^{-2}$$

is an effective area; $d_{k_\alpha(\omega)}^i(x,y)$ is the ith component of the displacement field for mode α at frequency ω and $n(x,y;\omega)$ is the material refractive index at frequency ω, both at waveguide
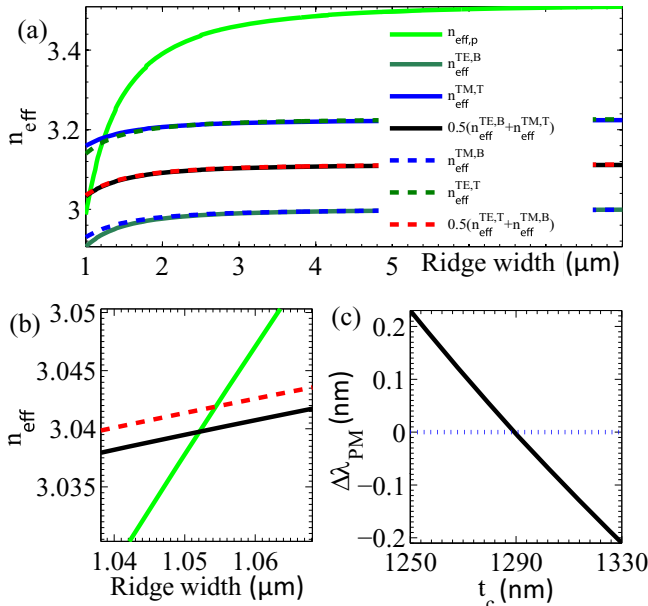

FIG. 2. (Color online) (a) Dependence of effective index of each mode on the ridge width; (b) the same as (a) but zoomed in around the cross points; (c) difference of PM wavelengths of the two SPDC processes as a function of the core thickness.

cross-sectional position (x, y), and we have chosen the mode amplitudes such that we can take the phase associated with the effective area to be zero [35].

Normalization of the quantum state $|II\rangle$ requires $\int d\omega_1 d\omega_2 \sum_{\alpha,\beta} |\phi_{\alpha\beta}(\omega_1, \omega_2)|^2 = 1$, which determines $|\nu|^2$. From the form of $|\Psi_{\text{gen}}\rangle$ we see that $|\nu|^2$ can be thought of as the average number of generated photon pairs per pump pulse. Note that the BWF is symmetric under exchange of both mode indices and frequencies $\phi_{\alpha\beta}(\omega_1, \omega_2) = \phi_{\beta\alpha}(\omega_2, \omega_1)$ but it does not necessarily possess any additional symmetry, i.e., $\phi_{\alpha\beta}(\omega_1, \omega_2) \neq \phi_{\beta\alpha}(\omega_1, \omega_2)$ and $\phi_{\alpha\beta}(\omega_1, \omega_2) \neq \phi_{\alpha\beta}(\omega_2, \omega_1)$.

In deriving Eq. (1), we have assumed that the only nonlinearity present is the one that results in photon pair generation and extends from $-L/2$ to $L/2$ in a channel structure that is otherwise linear. This simplifies the calculation, but neglects any coupling losses and facet reflections that would have to be included in a more realistic analysis. Here $\phi_P(\omega)$ is taken to identify the pump pulse at $t = 0$, with the pulse usually considered to be at the center of the nonlinear region. However, irrespective of the position of the pump pulse at $t = 0$, $\phi_{\alpha\beta}(\omega_1, \omega_2)$ specified by Eq. (2) describes the state at $t = 0$. If $\phi_{\alpha\beta}(\omega_1, \omega_2)$ is allowed to propagate far into the future *according to the linear dynamics only*, it will evolve into the actual BWF far in the future. In the terminology of scattering theory, $\phi_{\alpha\beta}(\omega_1, \omega_2)$ describes an asymptotic-out state. If we move the origin of coordinates to the output facet, and choose instead to specify the pump pulse at a time $T > 0$ before the time we specify the asymptotic-out state for the generated photons, we have

$$\Phi_{\alpha\beta}(\omega_1, \omega_2) = e^{i[k_\alpha(\omega_1) + k_\beta(\omega_2) - k_p(\omega_1 + \omega_2)]L/2} e^{-i(\omega_1 + \omega_2)T}$$
$$\times F_{\alpha\beta}(\omega_1, \omega_2)\Phi_P(\omega_1 + \omega_2),$$

where $\Phi_P(\omega) \equiv \phi_P(\omega) \exp[ik_p(\omega)L/2 + i\omega T]$ now characterizes the pump pulse with respect to the new origin and at a time $T > 0$ before the asymptotic-out BWF $\Phi_{\alpha\beta}(\omega_1, \omega_2)$, also specified with respect to the new origin. If we choose to specify $\Phi_{\alpha\beta}(\omega_1, \omega_2)$ to be at the new origin (the output facet) at $t = 0$ and wish to specify the pump pulse at the input facet, then T should be the transit time of the pump pulse in the nonlinear region.

The state given by $\Phi_{\alpha\beta}(\omega_1, \omega_2)$ is hyperentangled in frequency, polarization, and spatial mode. Since the photons are copropagating along the waveguide, paired photons need to be spatially separated if they are to be detected individually. One method is to use a 50:50 beamsplitter to separate the photons nondeterministically. However, only half of the photons can be used this way, as half of the time both photons will exit the same port instead of different ports. Alternatively, paired photons can be separated deterministically using one of the DOFs. For example, using a polarizing beamsplitter to separate the photons according to their polarizations, a spectral-modal hyperentangled state of the form [9]

$$|II_{\text{s-m}}\rangle = \frac{1}{\sqrt{2}} \int d\omega_1 d\omega_2 \Phi_{HB,VT}(\omega_1, \omega_2)|HB\omega_1, VT\omega_2\rangle$$
$$+ \Phi_{VT,HB}(\omega_1, \omega_2)|HB\omega_2, VT\omega_1\rangle$$
$$+ \Phi_{HT,VB}(\omega_1, \omega_2)|HT\omega_1, VB\omega_2\rangle$$
$$+ \Phi_{VB,HT}(\omega_1, \omega_2)|HT\omega_2, VB\omega_1\rangle$$

can be produced, where

$$|\alpha\omega_1, \beta\omega_2\rangle = \bar{a}_\alpha^\dagger(\omega_1)\bar{a}_\beta^\dagger(\omega_2)|\text{vac}\rangle,$$
$$\bar{a}_{\alpha(\beta)}^\dagger(\omega) = a_{\alpha(\beta)}^\dagger(\omega)e^{-ik_{\alpha(\beta)}(\omega)L/2},$$

with the overbars denoting that we have changed our origin of coordinates from that used in Eq. (1), as described above. If the paired photons were separated according to spatial modes instead, a spectral-polarization hyperentangled state

$$|II_{\text{s-p}}\rangle = \frac{1}{\sqrt{2}} \int d\omega_1 d\omega_2 \Phi_{HBVT}(\omega_1, \omega_2)|HB\omega_1, VT\omega_2\rangle$$
$$+ \Phi_{VTHB}(\omega_1, \omega_2)|HB\omega_2, VT\omega_1\rangle$$
$$+ \Phi_{HTVB}(\omega_1, \omega_2)|VB\omega_2, HT\omega_1\rangle$$
$$+ \Phi_{VBHT}(\omega_1, \omega_2)|VB\omega_1, HT\omega_2\rangle$$

could be generated.

Here we specifically analyze the generation of modal-polarization hyperentangled photons using a dichroic mirror or integrated dichroic splitter. The quantum state after passing an ideal dichroic mirror is given by

$$|II_{\text{m-p}}\rangle \simeq \int_0^{\omega_0} d\omega_i \int_{\omega_0}^\infty d\omega_s \Phi_{HBVT}(\omega_s, \omega_i)|HB\omega_s, VT\omega_i\rangle$$
$$+ \Phi_{VTHB}(\omega_s, \omega_i)|VT\omega_s, HB\omega_i\rangle$$
$$+ \Phi_{HTVB}(\omega_s, \omega_i)|HT\omega_s, VB\omega_i\rangle$$
$$+ \Phi_{VBHT}(\omega_s, \omega_i)|VB\omega_s, HT\omega_i\rangle, \quad (3)$$

where $\omega_0 = \omega_p/2$ is the splitting frequency. We have chosen to relabel the frequency variables as ω_s and ω_i, for the high- and low-energy photons (signal and idler photons), respectively, and we have neglected corrections arising because paired photons cannot be perfectly separated by the dichroic mirror for a generating pump pulse of finite bandwidth.

With the photons separated as in Eq. (3), we consider experiments sensitive only to the mode or polarization of the photons, and not their frequency. It can be shown (see the Appendix) that for this class of experiments, the quantum state in the polarization and spatial mode sub-space can be described by a density matrix, which in the basis $\{|HB, VT\rangle, |HT, VB\rangle, |VB, HT\rangle, |VT, HB\rangle\}$ can be written as

$$\rho_{\text{m-p}} = \begin{pmatrix} \sigma & \upsilon & \gamma & \delta \\ \upsilon^* & \epsilon & \zeta & \eta \\ \gamma^* & \zeta^* & \theta & \kappa \\ \delta^* & \eta^* & \kappa^* & \lambda \end{pmatrix}, \quad (4)$$

where

$$\sigma \equiv \int_0^{\omega_0} d\omega_i \int_{\omega_0}^\infty d\omega_s |\Phi_{HBVT}(\omega_s, \omega_i)|^2,$$

$$\upsilon \equiv \int_0^{\omega_0} d\omega_i \int_{\omega_0}^\infty d\omega_s \Phi_{HBVT}(\omega_s, \omega_i)\Phi_{HTVB}^*(\omega_s, \omega_i),$$

$$\gamma \equiv \int_0^{\omega_0} d\omega_i \int_{\omega_0}^\infty d\omega_s \Phi_{HBVT}(\omega_s, \omega_i)\Phi_{VBHT}^*(\omega_s, \omega_i),$$

$$\delta \equiv \int_0^{\omega_0} d\omega_i \int_{\omega_0}^\infty d\omega_s \Phi_{HBVT}(\omega_s, \omega_i)\Phi_{VTHB}^*(\omega_s, \omega_i),$$

TABLE I. Dispersion parameters of the down-converted modes in the design example.

	HB	VT	HT	VB
v (μm/ps)	84.9	86.5	85.8	86.0
D (10^2 ps/nm/km)	-8.31	-7.81	-5.98	-11.4

$$\epsilon \equiv \int_0^{\omega_0} d\omega_i \int_{\omega_0}^{\infty} d\omega_s |\Phi_{HTVB}(\omega_s,\omega_i)|^2,$$

$$\zeta \equiv \int_0^{\omega_0} d\omega_i \int_{\omega_0}^{\infty} d\omega_s \Phi_{HTVB}(\omega_s,\omega_i)\Phi_{VBHT}^*(\omega_s,\omega_i),$$

$$\eta \equiv \int_0^{\omega_0} d\omega_i \int_{\omega_0}^{\infty} d\omega_s \Phi_{HTVB}(\omega_s,\omega_i)\Phi_{VTHB}^*(\omega_s,\omega_i),$$

$$\theta \equiv \int_0^{\omega_0} d\omega_i \int_{\omega_0}^{\infty} d\omega_s |\Phi_{VBHT}(\omega_s,\omega_i)|^2,$$

$$\kappa \equiv \int_0^{\omega_0} d\omega_i \int_{\omega_0}^{\infty} d\omega_s \Phi_{VBHT}(\omega_s,\omega_i)\Phi_{VTHB}^*(\omega_s,\omega_i),$$

$$\lambda \equiv \int_0^{\omega_0} d\omega_i \int_{\omega_0}^{\infty} d\omega_s |\Phi_{VTHB}(\omega_s,\omega_i)|^2, \quad (5)$$

and $\sigma + \epsilon + \theta + \lambda = 1$.

For convenience, we expand the dispersion relation of each mode $k_q(\omega)$ ($q = \alpha,\beta$) about the splitting frequency ω_0, which is chosen as the degenerate PM frequency of the down-converted modes, yielding $k_q(\omega) = k_q(\omega_0) + (\omega - \omega_0)/v_q - \lambda_q^2/(4\pi c)D_q(\omega - \omega_0)^2$, where v_q designates the group velocity and D_q is the group velocity dispersion (GVD). These coefficients can be numerically calculated for our waveguide design, and their values are summarized in Table I. Additionally, we consider a narrow-band pump at twice the splitting frequency, i.e., $|\Phi_P(\omega)|^2 \approx \delta(\omega - 2\omega_0)$. In such a case, the pump pulse spectrum stays unchanged after propagating through the waveguide, and the phase term $-(\omega_s + \omega_i)T$ in $\Phi_{\alpha\beta}(\omega_s,\omega_i)$ is a constant. For a broadband pump pulse, however, its spectrum can be broadened and distorted by GVD and self-phase modulation, and the frequency-dependent phase in the BWF cannot be neglected [37]. Integrating over ω_i, we plot the spectral intensities $|\Phi_{\alpha\beta}(\omega_s,\omega_i)|^2$ and the associated phases, relative to the degenerate wavelength, of each of the four pieces of the BWF as functions of ω_s in Figs. 3(a) and 3(b), respectively, for a 2-mm-long waveguide. The distinct bandwidths are caused by the different group-velocity mismatch (GVM), $|1/v_\alpha - 1/v_\beta|$, values for each term, while the asymmetric behavior of the spectra is due both to nonzero GVMs and significant GVDs.

The differences in both the amplitude and phase of the four spectra can reveal which-process information, leading to a reduction in the visibility of a Hong-Ou-Mandel–type experiment. However, note that the spectra are nearly identical very close to ω_0. Thus we consider the effect of bandpass filters with a bandwidth B placed in two frequency bands, centered around $\omega_0 - \Delta$ and $\omega_0 + \Delta$, respectively, for removing the spectral distinguishability between the different terms in Eq. (3). Ideal rectangular-shaped filters restrict the bandwidth to $[\omega_0 - \Delta - B/2, \omega_0 - \Delta + B/2]$ for the
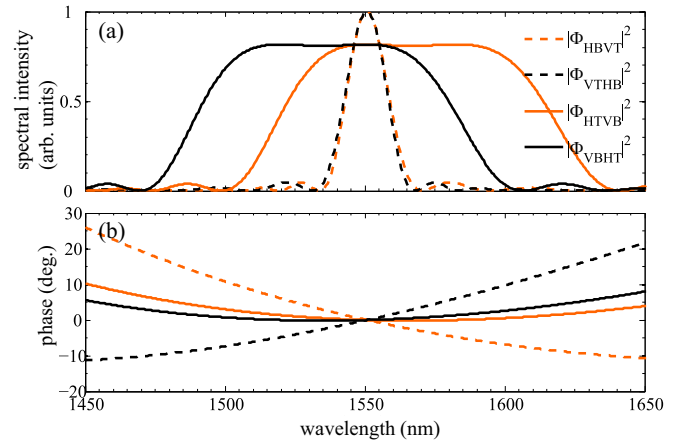

FIG. 3. (Color online) (a) Spectral intensities of the four terms in Eq. (3) and (b) the corresponding relative phases as functions of signal wavelengths using cw pump, i.e., $|\phi(\omega)|^2 = \delta(\omega - 2\omega_0)$.

low-frequency photon, ω_i, and $[\omega_0 + \Delta - B/2, \omega_0 + \Delta + B/2]$ for the high-frequency photon, ω_s. For filter bandwidths of 2 nm, 5 nm, and 10 nm, we plot the real and imaginary parts of the density matrix of the design example in Figs. 4(a)–4(c).

To characterize the degree of entanglement describing the generated state [Eq. (3)] for a given filter bandwidth, we calculate the maximum fidelity of the state with all maximally entangled states, or the *fully entangled fraction* (FEF) [38], which is given by

$$F = \max_{\psi,\varphi} \langle \Psi_{\text{ideal}}|\rho_{\text{m-p}}|\Psi_{\text{ideal}}\rangle, \quad (6)$$

where $|\Psi_{\text{ideal}}\rangle$ is the idealized maximally entangled polarization and mode hyperentangled state, which is given by

$$|\Psi_{\text{ideal}}\rangle = \tfrac{1}{2}(|H,V\rangle + e^{i\varphi}|V,H\rangle) \otimes (|B,T\rangle + e^{i\psi}|T,B\rangle). \quad (7)$$

In Eq. (6), the maximization is performed over all values of ψ and φ. In the case of $F = 1$, the generated state [Eq. (3)] is maximally entangled in polarization and spatial mode DOFs and behaves the same as the idealized state [Eq. (7)] with certain phase angles ψ and φ in any polarization and mode measurement [39].

The dependence of the FEF on the filter bandwidth is shown in Fig. 5. The corresponding FEFs for each filter bandwidth in Fig. 4 are calculated to be 0.99, 0.97, and 0.89, respectively. As expected, the FEF increases as the filter bandwidth decreases, indicating that the output state, Eq. (3), behaves more and more like the idealized state, Eq. (7), when subjected to measurements of polarization and mode. As a result, a high FEF can be obtained solely by bandpass filtering at the sacrifice of available photon pairs.

We emphasize that off-chip phase compensation is not required, contrary to other typical type-II processes in PPKTP and PPLN waveguides. This is because the GVM between paired photons in this platform is much lower than those obtained with birefringent materials, leading to much wider spectra and lower temporal walk off. Note that the spectrally narrower process 1 has a FWHM of ~30 nm, which is one order of magnitude larger than typical type-II SPDC bandwidths of PPKTP and PPLN waveguides.
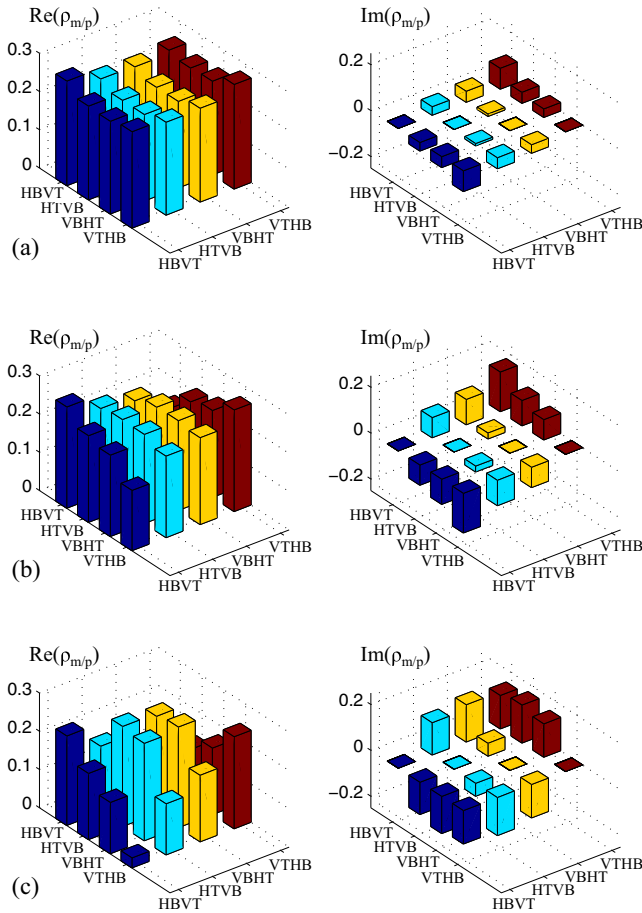
FIG. 4. (Color online) Real (left) and imaginary (right) parts of the filtered and normalized density matrices corresponding to Eq. (4) for a filter bandwidth of 2 nm, 5 nm, and 10 nm, respectively.

As an alternate strategy to filtering, the SPDC bandwidths could be increased by grading the modal indices along the propagation direction, for instance, by tapering the waveguide, in an approach similar to chirping the poling period in QPM [40]. However, if such a structure were used the which-process information from the phases of the pieces of the

BWF, such as in Fig. 3(b), could not be eliminated even if the spectral amplitudes had perfect overlap, due to the increased bandwidths. Therefore, the degree of hyperentanglement is not improved in a larger bandwidth unless off-chip phase compensations can be made simultaneously for the two type-II processes, which is not practical since each process has a different modal birefringence.

Finally, we calculate the generation rates of the two SPDC processes in a 2-mm-long waveguide; we find 1.9×10^{-9} and 8.3×10^{-9} pairs per pump photon for process 1 and process 2, respectively, over the whole spectral bandwidth, or 3.4×10^{3} and 2.7×10^{3} pairs/(s mW GHz) at the degenerate PM wavelength. The dependence of the available photon pairs per pump photon on the filter bandwidth are also shown in Fig. 5. With a filter bandwidth of 5 nm, the number of available photon pairs per pump photon are around 1.0×10^{-9} for both processes. These values are two orders of magnitude lower than a previously designed BRW [31] but are still comparable to those of bulk crystal SPDC sources.

The reason for the reduced efficiency is the poor modal overlaps, due to the use of the TE_{40} mode for the pump, as required by MPM. In principle, the modal overlaps and the efficiencies can be enhanced by a few orders of magnitude by using the fundamental mode as the pump, along with QPM instead of MPM, as in other studies [32]. In such a structure, concurrent PM can still be achieved by the same method described above. However, QPM in AlGaAs waveguides is far more challenging in terms of fabrication, and current techniques have not generated devices with low losses and high efficiencies compared to unpatterned waveguides [15]. On the other hand, we note the slightly unequal efficiencies degrade the degree of entanglement even with a very narrow filtering bandwidth. This problem could be addressed by modifying the epitaxial structure of the waveguide to try to achieve the same efficiency for the two processes [26].

V. CONCLUSION

We have presented a strategy for producing hyperentangled photons in semiconductor AlGaAs ridge waveguides. With the pump in the TE_{40} mode of a BRW, MPM can be achieved lithographically in deep etched ridge waveguides. Paired photons can be produced via two concurrent type-II SPDC processes. The two processes are phase matched at the same operating wavelength by choosing an appropriate waveguide core thickness. We specifically investigated the modal-polarization hyperentangled quantum state generated, using an ideal dichroic mirror to separate the paired photons, and calculated the density operator as well as the fully entangled fraction (FEF) as a measure of the degree of entanglement.

The calculations show that a high degree of hyperentanglement can be achieved with bandpass filtering of a few nanometers without off-chip phase compensation. It is worth noting that the modal entanglement achieved in our platform is provided by spatial modes with different guiding mechanisms, rather than the same kind of modes with different orders. Such a unique feature, which opens a way to generate hyperentanglement making use of the spatial DOF, might well provide extra control over the properties of the hyperentangled photons.
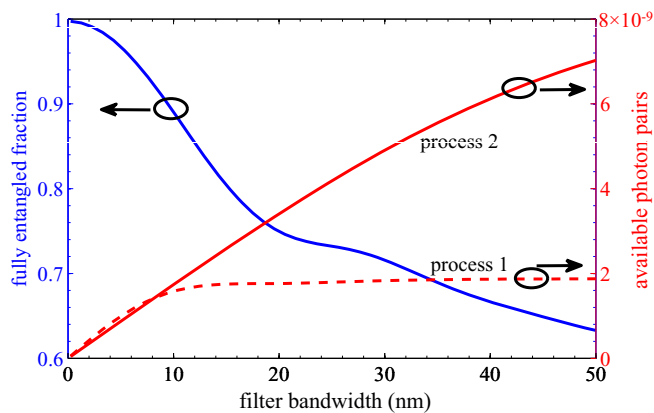

FIG. 5. (Color online) Dependences of the FEF and the numbers of available photon pairs per pump photon via the two processes on the filter bandwidth.

Since our strategy utilizes a III-V semiconductor platform, more advanced devices incorporating other functionalities can be envisioned, such as integrating diode lasers and passive structures such as dichroic splitters and bandpass filters. Therefore, this platform offers a path to realize an electrically pumped hyperentangled photon source.

APPENDIX

In this Appendix, we show that the result of a general (rank-1) polarization and mode measurement on the output state [Eq. (3)] is equivalent to a polarization and mode measurement on the density operator $\rho_{\text{s-m}}$ [Eq. (4)] that exists only in a polarization and mode subspace.

Consider the most general (rank-1) polarization and mode measurement that can be made on Eq. (3):

$$M = \text{Tr}(P\rho), \tag{A1}$$

where $\rho = |II_{\text{m-p}}\rangle\langle II_{\text{m-p}}|$ is the density operator and $P = |\psi\rangle\langle\psi|$ is the projection operator associated with the measurement, with

$$\begin{aligned}
|\psi\rangle = \int_0^{\omega_0} d\omega_i \int_{\omega_0}^{\infty} d\omega_s [Aa_{HB}^{\dagger}(\omega_s) + Ba_{HT}^{\dagger}(\omega_s) \\
+ Ca_{VB}^{\dagger}(\omega_s) + Da_{VT}^{\dagger}(\omega_s)][Ea_{HB}^{\dagger}(\omega_i) \\
+ Fa_{HT}^{\dagger}(\omega_i) + Ga_{VB}^{\dagger}(\omega_i) + Ha_{VT}^{\dagger}(\omega_i)]|\text{vac}\rangle.
\end{aligned} \tag{A2}$$

Here the complex coefficients satisfy the normalization condition $|A|^2 + |B|^2 + |C|^2 + |D|^2 = |E|^2 + |F|^2 + |G|^2 + |H|^2 = 1$. Similarly, the corresponding measurement made on $\rho_{\text{m-p}}$ is given by

$$M_{\text{m-p}} = \text{Tr}(P_{\text{m-p}}\rho_{\text{m-p}}), \tag{A3}$$

where $P_{\text{m-p}} = |\psi'\rangle\langle\psi'|$, and $|\psi'\rangle$ is given by

$$\begin{aligned}
|\psi'\rangle = (Aa_{HB}^{\dagger} + Ba_{HT}^{\dagger} + Ca_{VB}^{\dagger} + Da_{V,T}^{\dagger}) \\
\times (Ea_{HB}^{\dagger} + Fa_{HT}^{\dagger} + Ga_{VB}^{\dagger} + Ha_{VT}^{\dagger})|\text{vac}\rangle.
\end{aligned} \tag{A4}$$

With the parameters defined in Eq. (5), using Eqs. (A1)–(A4) and Eq. (3), we can prove $M = M_{\text{m-p}}$, i.e., the two states have the same measurement outcome in any polarization and mode measurement.

[1] J. T. Barreiro, N. K. Langford, N. A. Peters, and P. G. Kwiat, Phys. Rev. Lett. **95**, 260501 (2005).

[2] R. Ceccarelli, G. Vallone, F. De Martini, P. Mataloni, and A. Cabello, Phys. Rev. Lett. **103**, 160401 (2009).

[3] W. B. Gao, C. Y. Lu, X. C. Yao, P. Xu, O. Gühne, A. Goebel, Y. A. Chen, C. Z. Peng, Z. B. Chen, and J. W. Pan, Nature Phys. **6**, 331 (2010).

[4] H. Yan, S. Zhang, J. F. Chen, M. M. T. Loy, G. K. L. Wong, and S. Du, Phys. Rev. Lett. **106**, 033601 (2011).

[5] J. T. Barreiro, T. C. Wei, and P. G. Kwiat, Nature Phys. **4**, 282 (2008).

[6] M. Barbieri, F. De Martini, P. Mataloni, G. Vallone, and A. Cabello, Phys. Rev. Lett. **97**, 140407 (2006).

[7] T. Vértesi, S. Pironio, and N. Brunner, Phys. Rev. Lett. **104**, 060401 (2010).

[8] T. Suhara, Laser Photon. Rev. **3**, 370 (2009).

[9] M. F. Saleh, B. E. A. Saleh, and M. C. Teich, Phys. Rev. A **79**, 053842 (2009).

[10] M. F. Saleh, G. Di Giuseppe, B. E. A. Saleh, and M. C. Teich, IEEE Photon. J. **2**, 736 (2010).

[11] A. Christ, K. Laiho, A. Eckstein, T. Lauckner, P. J. Mosley, and C. Silberhorn, Phys. Rev. A **80**, 033829 (2009).

[12] P. J. Mosley, A. Christ, A. Eckstein, and C. Silberhorn, Phys. Rev. Lett. **103**, 233901 (2009).

[13] M. Karpiński, C. Radzewicz, and K. Banaszek, Opt. Lett. **37**, 878 (2012).

[14] S. V. Rao, K. Moutzouris, and M. Ebrahimzadeh, J. Opt. A: Pure Appl. Opt. **6**, 569 (2004).

[15] A. S. Helmy, P. Abolghasem, J. S. Aitchison, B. J. Bijlani, J. Han, B. M. Holmes, D. C. Hutchings, U. Younis, and S. J. Wagner, Laser Photon. Rev. **5**, 272 (2011).

[16] S. J. B. Yoo, R. Bhat, C. Caneau, and M. A. Koza, Appl. Phys. Lett. **66**, 3410 (1995).

[17] J. Ota, W. Narita, I. Ohta, T. Matsushita, and T. Kondo, Jpn. J. Appl. Phys. **48**, 04C110 (2009).

[18] S. J. Wagner, B. M. Holmes, U. Younis, I. Sigal, A. S. Helmy, J. S. Aitchison, and D. C. Hutchings, IEEE J. Quantum Electron. **47**, 834 (2011).

[19] T. W. Kim, T. Matsushita, and T. Kondo, Appl. Phys. Express **4**, 082201 (2011).

[20] M. Savanier, A. Andronico, A. Lemaître, E. Galopin, C. Manquest, I. Favero, S. Ducci, and G. Leo, Opt. Lett. **36**, 2955 (2011).

[21] D. Duchesne, K. A. Rutkowska, M. Volatier, F. Légaré, S. Delprat, M. Chaker, D. Modotto, A. Locatelli, C. De Angelis, M. Sorel, D. N. Christodoulides, G. Salamo, R. Arès, V. Aimez, and R. Morandotti, Opt. Express **19**, 12408 (2011).

[22] A. Orieux, A. Eckstein, A. Lemaître, P. Filloux, I. Favero, G. Leo, T. Coudreau, A. Keller, P. Milman, and S. Ducci, Phys. Rev. Lett. **110**, 160502 (2013).

[23] A. S. Helmy, Opt. Express **14**, 1243 (2006).

[24] R. Horn, P. Abolghasem, B. J. Bijlani, D. Kang, A. S. Helmy, and G. Weihs, Phys. Rev. Lett. **108**, 153605 (2012).

[25] S. V. Zhukovsky, L. G. Helt, D. Kang, P. Abolghasem, A. S. Helmy, and J. E. Sipe, Phys. Rev. A **85**, 013838 (2012).

[26] D. Kang and A. S. Helmy, Opt. Lett. **37**, 1481 (2012).

[27] J. Svozilík, M. Hendrych, and J. P. Torres, Opt. Express **20**, 15015 (2012).

[28] A. Vallés, M. Hendrych, J. Svozilík, R. Machulka, P. Abolghasem, D. Kang, B. J. Bijlani, A. S. Helmy, and J. P. Torres, Opt. Express **21**, 10841 (2013).

[29] R. T. Horn, P. Kolenderski, D. Kang, P. Abolghasem, C. Scarcella, A. D. Frera, A. Tosi, L. G. Helt, S. V. Zhukovsky, J. E. Sipe, G. Weihs, A. S. Helmy, and T. Jennewein, Sci. Rep. **3**, 2314 (2013).

[30] P. Yeh and A. Yariv, Opt. Commun. **19**, 427 (1976).

[31] S. V. Zhukovsky, L. G. Helt, P. Abolghasem, D. Kang, J. E. Sipe, and A. S. Helmy, J. Opt. Soc. Am. B **29**, 2516 (2012).

[32] J. Svozilík, M. Hendrych, A. S. Helmy, and J. P. Torres, Opt. Express **19**, 3115 (2011).

[33] P. Abolghasem and A. S. Helmy, J. Opt. Soc. Am. B **29**, 1367 (2012).

[34] S. V. Zhukovsky, D. Kang, P. Abolghasem, L. G. Helt, J. E. Sipe, and A. S. Helmy, Opt. Lett. **36**, 3548 (2011).

[35] Z. Yang, M. Liscidini, and J. E. Sipe, Phys. Rev. A **77**, 033808 (2008).

[36] L. G. Helt, E. Y. Zhu, M. Liscidini, L. Qian, and J. E. Sipe, Opt. Lett. **34**, 2138 (2009).

[37] For a 2 ps Gaussian pump pulse, GVD causes its duration to be doubled in ~14 mm.

[38] C. H. Bennett, D. P. DiVincenzo, J. A. Smolin, and W. K. Wootters, Phys. Rev. A **54**, 3824 (1996).

[39] Notice that the frequency dependent state [Eq. (3)] is not equivalent to the frequency independent state [Eq. (7)] even if the spectral indistinguishability is satisfied. For example, entanglement swapping requires spectral separability [see T. S. Humble and W. P. Grice, Phys. Rev A **77**, 022312 (2008)], which is not generally satisfied in [Eq. (3)].

[40] M. B. Nasr, S. Carrasco, B. E. A. Saleh, A. V. Sergienko, M. C. Teich, J. P. Torres, L. Torner, D. S. Hum, and M. M. Fejer, Phys. Rev. Lett. **100**, 183601 (2008).